PAPER

Non-linear MHD simulations of ELMs in JET and quantitative comparisons to experiments

IOP Publishing Plasma Physics and Controlled Fusion

Plasma Phys. Control. Fusion **58** (2016) 014026 (10pp) doi:10.1088/0741-3335/58/1/014026

Non-linear MHD simulations of ELMs in JET and quantitative comparisons to experiments

S Pamela[1], T Eich[2], L Frassinetti[3], B Sieglin[2], S Saarelma[1], G Huijsmans[4], M Hoelzl[2], M Becoulet[5], F Orain[2], S Devaux[6], I Chapman[1], I Lupelli[1], E Solano[7] and JET Contributors[8]

EUROfusion Consortium, JET, Culham Science Centre, Abingdon, OX14 3DB, UK
[1] CCFE, Culham Science Centre, Abingdon, Oxon, OX14 3DB, UK
[2] Max-Planck-Institut für Plasmaphysik, Boltzmannstrasse 2, D-85748 Garching bei München, Germany
[3] Tekes, VTT, PO Box 1000, 02044 VTT, Finland
[4] ITER Organization, Route de Vinon-sur-Verdon, CS90046, 13067 St Paul lez Durance, France
[5] CEA, IRFM, F-13108 Saint-Paul-lez-Durance, France
[6] Institut Jean Lamour, UMR 7198 CNRS—Université de Lorraine, Parc de saurupt, CS 50840, F-54011 NANCY Cedex
[7] LNF-CIEMAT, Madrid, Spain

E-mail: stanislas.pamela@ccfe.ac.uk

Received 24 June 2015, revised 2 October 2015
Accepted for publication 16 October 2015
Published 13 November 2015

Abstract

A subset of JET ITER-like wall (ILW) discharges, combining electron density and temperature as well as divertor heat flux measurements, has been collected for the validation of non-linear magnetohydrodynamic (MHD) simulations of edge-localised-modes (ELMs). This permits a quantitative comparison of simulation results against experiments, which is required for the validation of predicted ELM energy losses and divertor heat fluxes in future tokamaks like ITER. This paper presents the first results of such a quantitative comparison, and gives a perspective of what will be necessary to achieve full validation of non-linear codes like JOREK. In particular, the present study highlights the importance of pre-ELM equilibria and parallel energy transport models in MHD simulations, which form the underlying basis of ELM physics.

Keywords: MHD, edge-localised-modes, JOREK, JET, simulation, non linear

1. Introduction

In the absence of experimental scalings for ITER regarding edge-localised-mode (ELM) energy losses and resulting divertor heat fluxes in ITER-Like wall (ILW) conditions, simulations should be performed to provide alternative predictions for such ELM characteristics. To gain confidence in quantitative predictions of simulations for divertor heat fluxes in future devices like ITER, non-linear magnetohydrodynamic (MHD) codes like JOREK need to be validated against experimental data from current tokamaks. In recent years, qualitative comparisons with various diagnostics on different machines have confirmed that non-linear MHD simulations can reproduce experimental observations of ELMs with satisfying accuracy [1–3]. Key features of ELM dynamics, like the pedestal filamentation, the poloidal rotation of filaments, divertor heat flux profiles, precursors, and energy losses, are qualitatively well described by the current JOREK model.

Achieving quantitative predictions for future devices, however, requires a considerable extension of these qualitative comparisons toward systematic quantitative validation of simulations against experiments. The ability to predict ELM

[8] See appendix of [38].

energy losses and divertor heat fluxes in ITER—and eventually DEMO—relies on the demonstration that simulations can reproduce these key characteristics of ELMs for all possible experimental conditions in all actual machines. Namely, for all possible combinations of major radius, aspect ratio, plasma current, magnetic field, collisionality, pedestal pressure, gas injection, heating power, wall material, impurities etc.

The path to such extensive quantitative validation lies in the progressive construction of a large database for each current tokamak. This paper presents a first set of JET ILW experiments that were collected to begin this database. The ILW has a beryllium main-chamber wall, bulk-tungsten for the horizontal divertor target, and tungsten-coated CFC for the rest of the divertor [4]. Confinement and ELMs have been observed to be significantly different with the ILW than with the previous carbon wall [5]. The unseeded (i.e. no nitrogen seeding) pulses were chosen for the combination of good electron density and temperature measurements with the high-resolution Thomson scattering (HRTS), as well as infra-red (IR) measurements of the heat fluxes on the horizontal target of the outer divertor [6–10]. Following a brief description of the non-linear MHD model used in JOREK, we detail how experimental data was used to produce simulation input. The first simulation results using this initial database, together with their comparison to experimental data, represent the main achievement of this paper. Significant progress has been made in terms of ELM simulations, now producing ELMs of size and duration similar to experimental observations. The quantitative comparisons with the experiments reveals that simulations can reproduce quite accurately the ELM energy losses measured in experiments, which is the first time such a result has ever been obtained by a non-linear MHD code. However, there is some discrepancy in the way energy is transported to the divertor at low collisionality levels. In the conclusion, a discussion is proposed about how the present study and/or the JOREK model could be improved to resolve this discrepancy.

2. The non-linear MHD code JOREK

The 3D non-linear MHD code JOREK was initially developed with the aim of producing ELM simulations [11, 12]. The MHD model used here is described in previous ELM studies [1–3, 13–16]. It is a reduced MHD model for the five variables ψ (poloidal magnetic flux), Φ (electric potential), $v_{//}$ (parallel velocity), ρ (mass density), T (temperature). This reduced MHD model, first derived by Strauss [17, 18], assumes that the perpendicular velocity lies in the poloidal plane, which reduces the momentum equation to two variables (for $v_{//}$ and Φ), and that the toroidal magnetic field is constant in time.

The perpendicular mass and thermal diffusivities $D_\perp$ and $\kappa_\perp$ used in simulations are ad hoc coefficients with a well at the pedestal region to represent the H-mode transport barrier, as in [2]. The Spitzer resistivity is used as $\eta = \eta_o\ (T/T_o)^{-1.5}$, T_o being the temperature at the magnetic axis. Likewise, a temperature-dependent perpendicular viscosity is assumed: $\mu = \mu_o\ (T/T_o)^{-1.5}$. And the Braginskii model [19] is used for parallel thermal conductivity: $\kappa_{//} = \kappa_o\ (T/T_o)^{2.5}$.

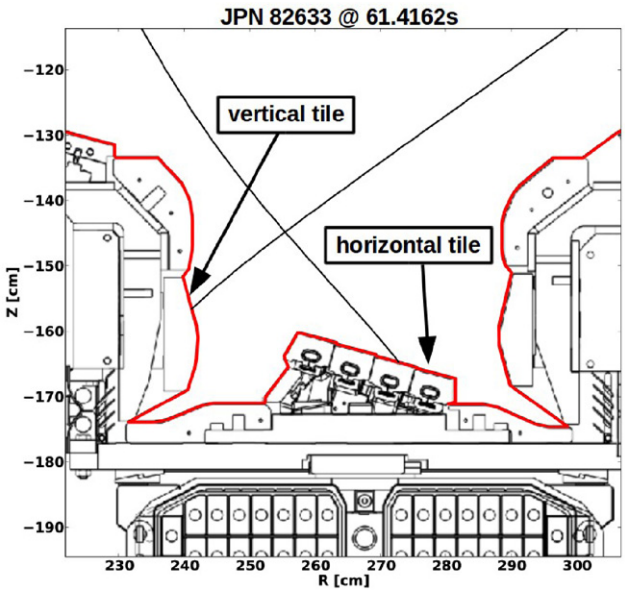

Figure 1. The JET ILW showing the separatrix of the plasma shape used for all selected pulses, with the inner strike point on the vertical target (tile-3) and the outer strike point on the horizontal target (tile-5).

The plasma boundary in the scrape-off layer (SOL) is a flux surface, on which Dirichlet boundary conditions (zero perturbation) are applied for all variables except density and temperature. For density and temperature, Neumann conditions with null gradient are applied. At the divertor targets, Mach-1 (or Bohm) boundary conditions are used for the parallel velocity, which is equivalent to setting the parallel velocity to the temperature dependent sound speed $v_{//} = c_s = (5/3\ T/m_i)^{1/2}$. Temperature and density have free outflow boundary conditions at the target, without density reflection (i.e. no recycling). In the private region, which is also bounded by a flux surface, Dirichlet conditions are used for all variables.

The 2D poloidal grid is composed with isoparametric cubic Bezier finite elements [12], so that continuity is satisfied for all variables, including the R, Z-coordinates. The finite element grid is aligned to equilibrium flux surfaces for the three regions of the core, the SOL and the private region. Alignment along open flux surfaces in the SOL is important in order to accurately treat the fast parallel transport of energy along magnetic field lines (i.e. the heat flux $\kappa_{//} \nabla_{//} T$). The toroidal dimension is represented by a Fourier series. The time stepping is done using the implicit Crank–Nicolson scheme, so that the size of time steps depends only on the time scale of the instabilities that are simulated (i.e. not the space grid resolution).

3. The choice of pulses and simulation parameters

Initially, four JET ILW unseeded pulses were selected to provide a scan in the edge safety factor q_{95}, with varying plasma current at constant field: discharges 82893, 82897, 82898 and 82900 had a q_{95} of 3, 3.9, 4.9 and 6.1 respectively. The objective was to investigate the effect of connection length on the energy transport from the pedestal to the divertor. These

Table 1. List of JET ILW pulses used for simulations.

Pulse	Time range	B_Φ [T]	I_P [MA]	q_{95}	NBI [MW]	N_e^{pad} [m^{-3}]	T_e^{pad} [keV]	ν_{e*}^{pad}
82630	[60.0, 63.0]	2.0	2.0	3.15	12	5.2×10^{19}	0.50	0.90
82631	[55.9, 58.1]	2.0	2.0	3.15	11	5.7×10^{19}	0.37	1.80
82633	[61.0, 62.0]	2.0	2.0	3.15	10	6.0×10^{19}	0.20	6.47
82634	[59.5, 60.5]	2.0	2.0	3.15	10	5.7×10^{19}	0.38	1.70
82635	[57.5, 58.5]	1.3	1.3	3.15	6.6	3.8×10^{19}	0.40	1.02
82636	[60.5, 61.0]	1.6	1.6	3.15	11	4.3×10^{19}	0.52	0.69
82637	[60.3, 61.7]	1.0	1.0	3.15	8	3.4×10^{19}	0.20	3.67
82638	[57.5, 58.5]	2.0	2.0	3.15	9.8	5.8×10^{19}	0.50	1.00
82642	[55.4, 57.8]	2.0	2.0	3.15	9.6	6.0×10^{19}	0.48	1.12
82643	[55.5, 57.9]	2.5	2.5	3.15	10	6.7×10^{19}	0.65	0.68
82644	[55.6, 56.6]	2.5	2.5	3.15	10	6.5×10^{19}	0.64	0.68
82893	[55.1, 56.2]	2.4	2.5	3.03	13	6.4×10^{19}	0.56	0.85
82897	[59.8, 60.8]	2.4	2.0	3.85	13.5	4.3×10^{19}	0.63	0.57
82898	[59.7, 62.7]	2.4	1.6	4.9	13.5	2.9×10^{19}	0.70	0.40
82900	[62.2, 63.2]	2.4	1.3	6.1	12.5	2.0×10^{19}	0.80	0.26
83330	[56.2, 57.3]	2.0	2.0	3.15	21	3.7×10^{19}	0.90	0.20
83331	[55.3, 56.8]	2.0	2.0	3.15	21.5	3.4×10^{19}	0.95	0.16
83333	[56.0, 56.9]	2.4	2.4	3.15	25	4.0×10^{19}	1.10	0.14
83334	[54.7, 55.3]	2.4	2.4	3.1	25	4.8×10^{19}	1.15	0.15
83337	[56.2, 57.2]	1.6	1.6	3.15	15	3.9×10^{19}	0.67	0.37
83338	[55.5, 56.5]	1.6	1.6	3.15	18	3.0×10^{19}	0.83	0.19
83339	[55.5, 56.5]	1.3	1.3	3.15	15	2.4×10^{19}	0.67	0.23
83340	[52.7, 53.5]	2.8	2.8	3.1	25	6.5×10^{19}	0.80	0.43
83341	[54.1, 55.1]	2.8	2.8	3.1	25	4.9×10^{19}	0.90	0.26
83432	[56.2, 56.8]	2.4	2.4	3.15	23	4.0×10^{19}	1.10	0.14
83438	[55.6, 56.7]	2.4	2.4	3.15	23	4.0×10^{19}	1.10	0.14
83562	[50.0, 53.5]	2.0	2.0	3.17	11.7	5.1×10^{19}	0.60	0.62

particular pulses were chosen because they all had the IR camera on the outer divertor, with the strike point positioned in the middle of the divertor. This would permit direct comparisons of ELM divertor heat fluxes between simulations and experiments. The other, most important characteristic of these pulses was that the HRTS diagnostic was available, so that pre-ELM electron density (n_e) and temperature (T_e) profiles were available. The reconstruction of these profiles with respect to the magnetic equilibrium is described in [6–8]. The n_e and T_e profiles are needed to compute the Grad–Shafranov equilibria for the simulations, because the poloidal finite-element grid is aligned to the Grad–Shafranov equilibrium for each pulse.

Although the simulations of the q_{95} scan produced interesting results, it rapidly became evident that four pulses were not enough to bring weight to the simulation results. Further, by using real experiments, the q_{95} scan is polluted by other variations from pulse to pulse, such as different pedestal pressure levels. This brought the decision to undertake a broader approach of simulating experiments, using a larger array of pulses. A total of 27 ILW pulses were retained.

All pulses were selected using these same two criteria: availability of HRTS profiles and IR camera data with the outer strike point on the vertical target (or tile-5). Figure 1 shows the divertor of the ILW on JET, together with the separatrix of pulse 82633. All plasmas had the same shape (low triangularity) with the inner strike point on the vertical target (tile-3) and the outer strike point on the horizontal target (tile-5). The field ranges from 1 T to 2.5 T, and the plasma current from 1 MA to 2.8 MA. Table 1 provides the list of pulses with their main characteristics, including the pedestal neoclassical collisionality calculated, as in [7], as $\nu_{e*}^{ped} = q_{95} R^{2.5} a^{-1.5} \lambda_{ee}^{-1}$, where $\lambda_{ee} = 1.7 \times 10^{17} (T_e^{pad})^2 (n_e^{pad})^{-1} (\ln \Lambda)^{-1}$ is the electron–electron Coulomb collision mean free path (T_e in eV). R and a are the major and minor radii respectively, and $\ln(\Lambda)$ is the Coulomb logarithm. It should be noted that the pedestal pressure scales almost linearly with plasma current for these pulses, as seen from figure 2. Not all pulses are linearly unstable with respect to ideal MHD. Some pulses lie beyond the stability threshold, while some lie largely inside. Figure 2 includes the critical pedestal pressure values at which each pulse would be ideally unstable, as calculated self-consistently by the HELENA code, when increasing the pedestal pressure and the bootstrap current accordingly [20].

The process to go from experimental data to simulation involves the production of pre-ELM n_e and T_e profiles using the HRTS diagnostic for the computation of the JOREK Grad–Shafranov equilibria. These profiles are projected on the poloidal flux grid given by the magnetic equilibrium calculated by EFIT. For the total pressure, the ion temperature T_i is assumed equal to the electron temperature T_e. Since the magnetic-only EFIT reconstruction is generally misaligned with most diagnostics, the HRTS profiles are shifted using the

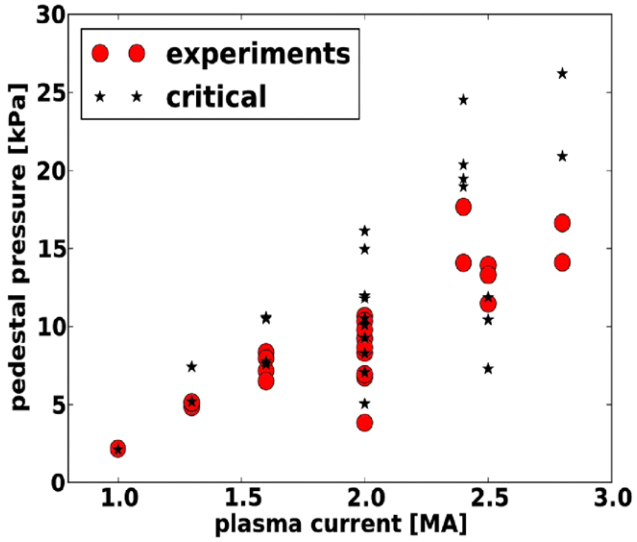

Figure 2. The pedestal pressure p_{PED} as a function of the plasma current I_{P} for the JET pulses incorporated into the simulation database, including the critical p_{PED} values at which the ideal peeling-ballooning stability boundary is crossed.

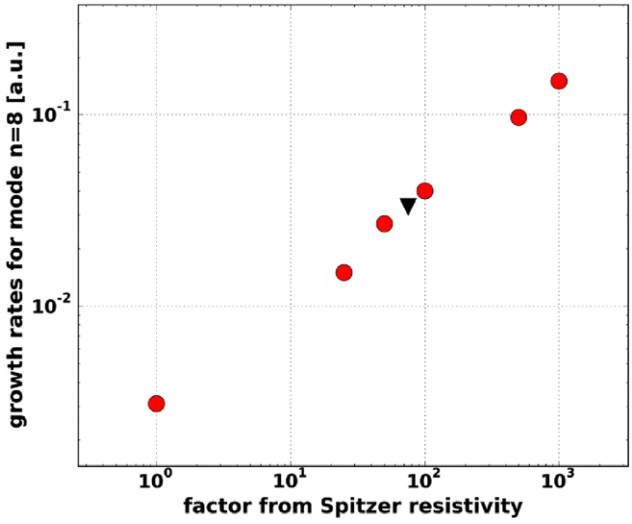

Figure 3. Growth rates of the mode $n = 8$ for the pulse 82630 as a function of resistivity. The black triangle is the resistivity value at which all simulations were run (75 η_{Spitzer})

power flow formula for the upstream temperature, as given by equation (1) in [21]. The EFIT reconstruction is used to provide the boundary condition (on ψ) and the FF' profile to solve the Grad–Shafranov equation. The magnetic-only equilibria from EFIT do not have any edge current, so that in order to include the bootstrap current in simulations, the FF' profile is modified to satisfy both the bootstrap current in the pedestal (using the Sauter model [22]) and the total plasma current. For each pulse, it is ensured that the JOREK Grad–Shafranov equilibrium has the accurate total plasma current I_{P}, pedestal bootstrap current, q_{95} and separatrix position (with respect to the EFIT separatrix).

A first set of simulations was run for the initial q_{95} scan using diamagnetic terms, but the diamagnetic effects were dropped for the full database simulations. The main reason for this approximation is that it is numerically challenging at present to run simulations with close-to-experimental resistivity including diamagnetic terms, which induce thin current layers that are numerically unstable at low resistivity. As has been shown in previous ELM studies [1], having near-experimental resistivity values is critical to bring simulations closer to experimental observations, since ballooning modes in a resistive regime do not give a good representation of type-I ELMs. Hence, for the present study it was estimated that simulations would benefit more from a low resistivity without diamagnetic effects rather than the opposite.

The resistivity used for the simulations was taken a factor 75 from the exact Spitzer resistivity. The parallel conductivity coefficient κ_{o} used for the Braginskii term $\kappa_{//} = \kappa_{\mathrm{o}}\ (T/T_{\mathrm{o}})^{2.5}$ was taken a factor 8 below the exact Braginskii electron coefficient (hence a factor ~5 above the ion Braginskii coefficient). The viscosity was $\mu = 5 \times 10^{-8}$ kg m^{-1} s^{-1}. The pedestal perpendicular diffusivity and conductivity were $D_{\perp} = 0.5$ m^{2}s^{-1} and $\kappa_{\perp} = 5 \times 10^{-9}$ m^{-1} s^{-1}. These choices of MHD parameters are a result of preparatory tests to ensure that most simulations would succeed without numerical difficulty. A single toroidal Fourier mode $n = 8$ was used.

JOREK simulations with a large number of toroidal harmonics are possible [23, 24] but these large-scale simulations require significant super-computer resources. At the moment, it is not feasible (within the available computational resources) to venture into such advanced simulations for all the discharges in the present JET database—not without certainty that the physics outcome of such simulations will be quantitatively satisfying. The present study required three months of simulation on HELIOS (Japan-JAEA). About six to nine months would be necessary to run the same simulations with multiple harmonics, and thus it is necessary to ensure that such simulations would be as optimized as possible, with respect to experiments, by first using single-harmonic simulations. It is most important to note that the simulation time itself, would be similar for higher n-mode simulations, the jump from 3 to 9 months simply comes from the longer queuing time required for larger simulations on super-computers. There is a large misunderstanding in the fusion community between the ability to run one large (high resolution) simulation, given the size of modern CPU machines, and the practical ability to run several hundreds of these simulations per year in order to gain a physics understanding of the immediate relevant issues. This should improve in future years, as large super-computers become more frequently available.

Although the reason for using a resistivity 75 times higher than the experimental Spitzer value is simply numerical, it is expected that higher resistivity enhances the growth rates of the ballooning modes, and can therefore lead to higher pedestal energy losses. Figure 3 shows a scan in resistivity for the mode $n = 8$ for pulse 82630. The growth rates are observed to be clearly affected by resistivity, but it is not evident that the simulation domain lies in a well-defined resistive regime compared to the Spitzer resistivity case. As progress is made, simulations will eventually be possible at the exact Spitzer values. For the present study, it should be kept in mind that

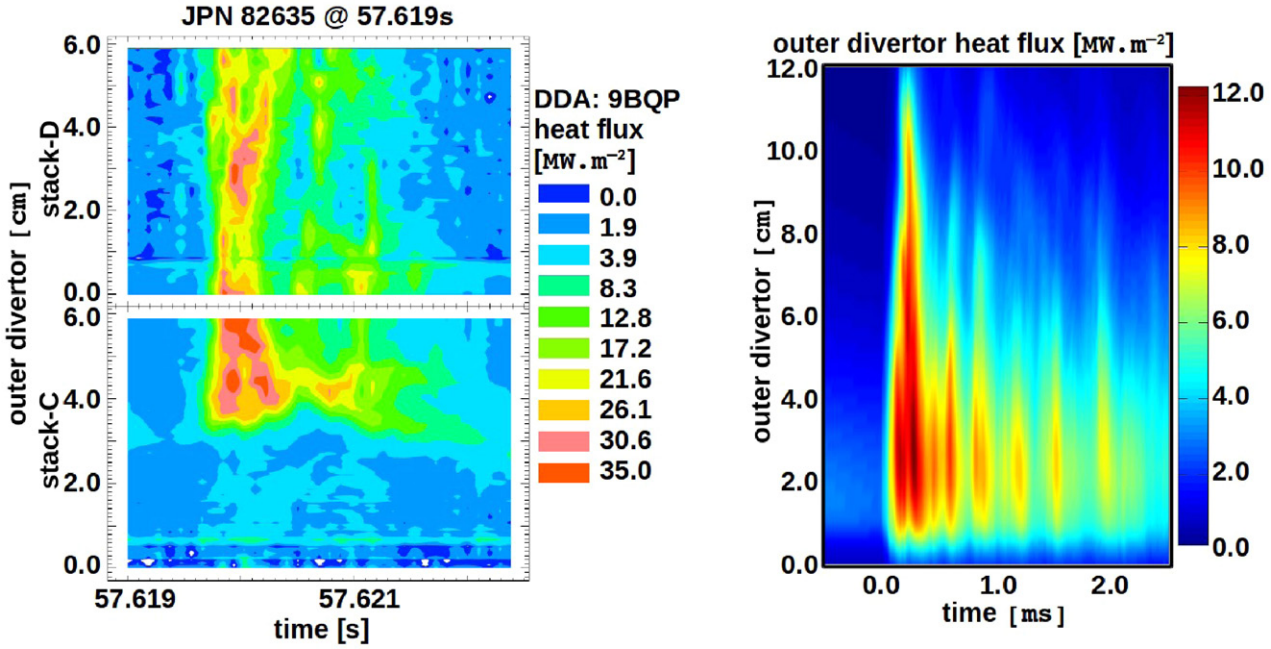

Figure 4. *Left:* Outer divertor heat flux observed on the infra-red camera of JET for pulse 82635. *Right:* Outer divertor heat flux from simulation of pulse 82635. The same time and length scales have been used for both plots. The Stacks C and D are the 3rd and 4th blocks of the horizontal target, as shown in figure 1.

the resistivity is not as low as it should be, which can affect simulation results.

4. Simulation results: main characteristics

Before comparing simulation results to experimental data, it is important to focus on certain details of these results as they stand, and more importantly, on how they compare to previous results. While, as will be shown in next section, some aspects of the results fail to align with the experimental observations, this set of simulations represents a significant improvement with regards to previous studies [1]. Some questions and doubts about general features of ELM simulations with the JOREK code that had long remained unanswered are now clarified.

Simulations were successfully produced for several experiments, using low resistivity (a factor 75 above the Spitzer values) and low viscosity. Previous simulations had been run with low resistivity only, the present study demonstrates that low viscosity is just as important. Focusing efforts on lowering viscosity and resistivity towards experimental values brings improvements to simulations that cannot be achieved by advanced MHD models alone. Of course, the opposite is also true—for example, diamagnetic effects largely improve the inboard/outboard balance of divertor heat fluxes caused by ELMs [25], which was not captured in the present simulations. Prediction models for ITER and DEMO will require diamagnetic drifts, neoclassical viscosity, advanced (eg. kinetic) parallel conductivity models and possibly full (non-reduced) MHD. However, with or without these, simulations will need to run at experimental resistivity and low viscosity.

The first and main improvement from previous works is the time scale and size of the simulated ELMs: rather than short, small bursts ($\tau_{\mathrm{ELM}} < 300$ μs and $\Delta W_{\mathrm{ELM}} < 2\%$) when only low resistivity was used in the past, simulated ELM crashes here with lower viscosity are longer and larger ($\tau_{\mathrm{ELM}} = 3$ ms and $\Delta W_{\mathrm{ELM}} = 4.9\%$ on average). This is particularly important for the present study, done using ILW pulses, which have longer (slower) ELMs than with the previous Carbon wall [5]. It should be noted that in this paper the time duration of an ELM is defined as the trace of the heat flux on the outer divertor (as opposed to the MHD duration of the instability). Also, ΔW_{ELM} is defined relative to the total plasma energy: $\Delta W_{\mathrm{ELM}} = W_{\mathrm{ELM}} / W_{\mathrm{TOT}}$. Figure 4 shows an ELM for pulse 82635, as seen with the heat flux on the outer divertor, using the IR camera, and its simulation. It is worth noting that there is an extremely large array of heat flux patterns, both in the simulations and in the experiments, with variations in spacial and temporal evolution, with repetitive or singular deposition peaks, with isolated 'blobs' etc. The study of all these different patterns, experimentally or from simulations (with or without comparison), would be quite vast if in detail and thus would certainly require a dedicated publication. Until more advanced simulation results are obtained, such detailed studies of the simulated heat fluxes is left for future times. Eventually, the study of simulated heat fluxes on the divertor should be compared against experiments as well as other simulation models, fluid and kinetic [26–29].

The second improvement in comparison to older JET simulations is that the width of divertor heat flux profiles is closer to experiments. At higher resistivity and/or higher viscosity, it is systematically greater than 15 cm, which is larger than the experimental IR observations. In the present simulations, the heat flux profile width ranges from 8 cm to 16 cm, averaging at 11.5 cm between all pulses. The heat flux profile widths cannot be extracted from the IR data for most pulses because

part of the profiles are beyond the edge of the target plate, as seen on figure 4 (left), but many pulses clearly do have a profile width $\leqslant$12 cm.

Another feature of ELMs that has successfully been reproduced by simulations is the presence of long-lasting precursors before some of the ELM crashes [1]. Such a precursor had been observed only once before in simulations, and the present database produced two, meaning precursors are a reproducible feature of ELMs in low resistivity simulations. The simulated pulses 82893, 83333 have precursors of 0.7 ms and 1.5 ms respectively, which are traceable on the divertor heat flux before the main crash appears. However, these two pulses do not exhibit such precursors in the experiments on the IR camera. And conversely, pulses that had precursors in the experiments did no have precursors in the simulations.

Out of the 27 pulses, only 4 pulses had experimental precursors observable on the IR data: pulses 82631, 82634, 83338 and 83339. Hence any conclusion about the dependence of such precursors on plasma parameters is not straightforward. Experimental precursors can last as long as the main ELM crash, with heat fluxes as high as 70% of the peak heat flux of the main ELM crash, but with a much smaller wetted area (typically less than half of the main crash). Some precursors have stripes moving radially with time, others are just intermittent bursts of heat flux increasing progressively until the main crash. Detailed studies of ELM precursors on the divertor and their relation to magnetic perturbations and pedestal n_e and T_e profiles should be attempted in near future. Any experimental understanding of ELM precursors would strongly benefit the theoretical understanding of ELMs and therefore modelling.

The origin of precursors in simulations is also not well understood, apart from the fact that low resistivity is required, but they are a sign that simulations are becoming experimentally relevant. In particular, they will be of importance when exploring multiple ELM cycles and the crossing of the peeling-ballooning stability limit, since they demonstrate that unstable modes can remain at low activity in the pedestal for extended periods of time before producing an ELM crash. In addition, simulations with precursors have much more violent ELM crashes, which could be considered as the most important theoretical feature of this study. All other simulated ELMs have peak heat fluxes lower than 91.4 MW m^{-2} on the outer divertor (with an average of 34.2 MW m^{-2}), except for these two pulses that have precursors: 290 MW m^{-2} and 193.5 MW m^{-2} respectively. Unfortunately, this also means that these pulses are numerically more challenging. Pulse 82893 had numerical instabilities that prevented the simulation from passing the main non-linear phase, while pulse 83333 only succeeded for about 0.5 ms of the ELM crash, as seen on figure 5, before it became numerically unstable. Thus, the ELM duration and ELM size was not available for these simulations.

Some theoretical explanations have been proposed in [30]: that precursors are due to the stabilising influence of the strong shear near the *X*-point inside the separatrix, which could explain the disappearance of precursors at higher resistivity. Although it is yet too early to make any clear comparison,

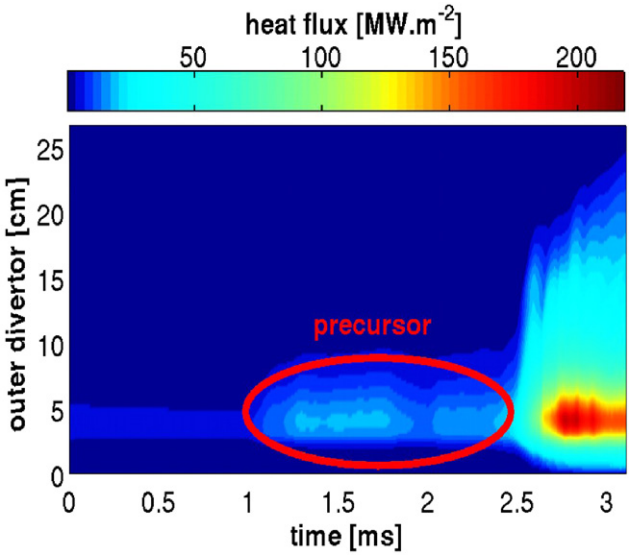

Figure 5. Outer divertor heat flux for pulse 83333 showing a precursor to the ELM. The simulation becomes numerically unstable at a later stage. Simulations with precursors have much larger crashes than those without precursor.

further simulation works on precursors should include a study of the effect of the *X*-point magnetic shear to explore this interpretation. In particular, it should be noted that in high-resistivity simulations, the ballooning modes are always active, no matter what the pedestal pressure gradient is, such that the size of the ELM crash is proportional to the linear growth rate of the modes. In the low resistivity simulations presented here, however, all simulations have comparable growth rates (within one order of magnitude), and the two pulses with precursors are neither the most nor the least linearly unstable. However, when the ballooning mode starts interacting with the background equilibrium during the precursor, it is clearly not evacuating as much density and energy as it should (compared to other pulses with similar linear growth rates), suggesting that it is stabilised by the background equilibrium. Nevertheless, this damped mode eventually creates a crash much larger than all other cases without precursors (including those with higher linear growth rates). In addition, although the present simulations did not include diamagnetic drifts, a strong flow shear is still present in the pedestal, due to the pedestal pressure gradients and the *X*-point geometry (see [31] for detailed studies of equilibrium flows in simulations). It is quite certain that the equilibrium pedestal flow also has a strong influence on the linear and non-linear stability of the ballooning modes, and should also be considered in further studies of precursors, with and without diamagnetic drifts.

Finally, q_{95} could play a role in the intensity of the divertor heat fluxes. For the shortest field lines starting inside the hot pedestal (at least $^1/_2 T_{PED}$), the connection length, calculated as half the length of the field line from inner to outer divertor target, increases from 215 m at $q_{95} = 3$ up to 295 m at $q_{95} = 6.1$. Note that this is about a factor 5 higher than the estimate $\pi\, R\, q_{95}$, which is consistent with the assumption required by kinetic simulations of parallel ion transport [29]. The peak heat flux on the outer divertor is seen to decrease

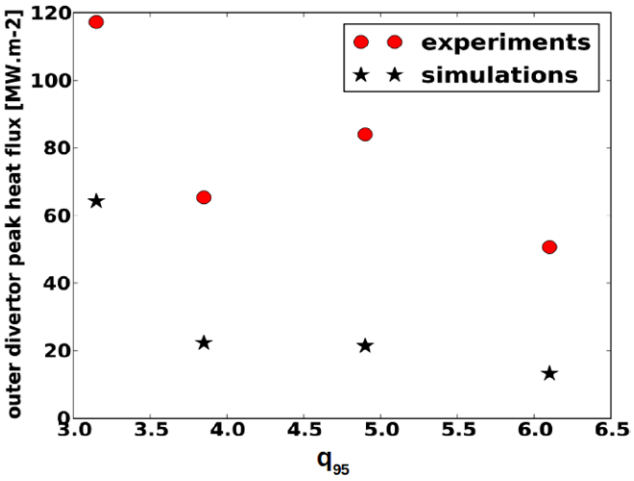

Figure 6. The outer divertor peak heat flux as a function of q_{95}.

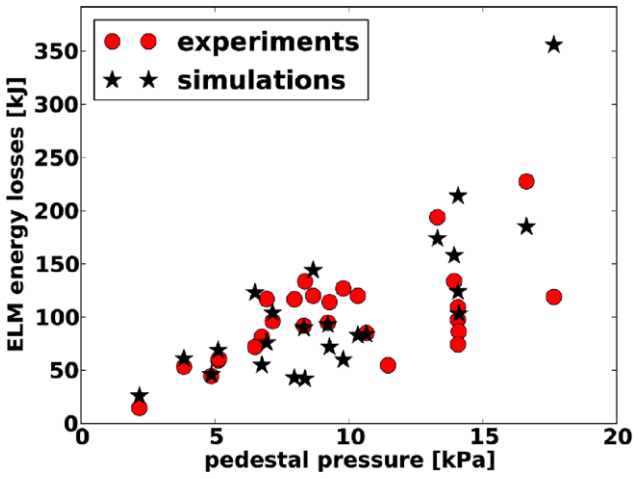

Figure 7. ELM energy losses increase with pedestal pressure. The simulation results agree relatively well with the experimental data.

from 64.3 MW m^{-2} at $q_{95} = 3$–13.2 MW m^{-2} at $q_{95} = 6.1$, as seen in figure 6. Although the trend is similar in experiments and simulations, the peak heat flux is much higher in the experiments, up to a factor 5. More details on comparison of heat fluxes between simulations and experiments are given in next section. Despite the agreement that heat fluxes are lower at higher q_{95}, there is also evidence, as will also be seen in the next section, that peak heat fluxes on the divertor increase at higher plasma current (and consequently higher pedestal pressure, as seen from figure 2). Hence, although longer transport time along field lines is required for energy to travel from the pedestal to the divertor, the decrease of divertor heat fluxes at higher q_{95} might simply be a result of lowering the plasma current and pedestal pressure. Nonetheless, the MHD model used for this study does not include neutrals, with which radiation and charge exchange would affect energy flowing along field lines in the SOL: longer travel time along field lines would result in lower divertor heat fluxes [32].

5. Comparison against experimental data

The first aspect of ELMs to consider is the energy loss, ΔW_{ELM}. This increases with p_{PED}, both in the experiments and in the simulations, which agree very well, as shown in figure 7. The ELM energy losses also increase with plasma current, but this dependence on I_{P} is only due to the increase in pedestal pressure at higher plasma current, as shown in figure 2. While integration of the plasma energy and the divertor heat loads is straightforward in the simulations, experimentally it was calculated using the HRTS diagnostic, with averaged pre- and post-ELM profiles. This method to calculate W_{ELM} values using HRTS has been shown to be in good agreement with the diamagnetic energy estimates (W_{DIA}) from EFIT for carbon-wall data [6–8].

While this comparison seems consistent, the main interest lies in how energy is transported from the pedestal to the divertor. This is done by comparing the peak heat flux on the outer divertor with IR data, which is illustrated on figure 8. Note that each IR data has been averaged for 20–50 ELMs around the time selected for simulations. The simulated heat flux is regularly lower than the IR observations. This could be due to the fact that the coefficient for the heat flux $\kappa_{//} = \kappa_{\mathrm{o}} (T/T_{\mathrm{o}})^{2.5}$ was lower than the Braginskii electron value. Note that high $\kappa_{//}$ values are numerically challenging, and some pulses that had numerical instabilities are not presented here due to such problems (except pulsed 82893 and 83333 due to their precursor). Taking $\kappa_{//}$ to higher values will require additional efforts and is left for future work. However, this difference between the simulated and the experimental peak heat flux increases further at higher pedestal pressure, even though the simulated energy losses become larger like in the experimental observations. What compensates the lower heat fluxes in simulations is not the width of heat flux profiles, which in fact decreases at higher pedestal pressure, it is the duration of the ELMs: they are not as intense as the experimental ELMs, but last longer in order to evacuate the excess plasma pressure. This is clearly seen as a function of pedestal collisionality $\nu_{\mathrm{e}*}^{\mathrm{ped}}$, in figure 8. In the experiments, the ELMs become more intense and shorter at low $\nu_{\mathrm{e}*}^{\mathrm{ped}}$, while in simulations, they become a little more intense, but last much longer, which results in similar total energy losses. Note that this decrease in ELM duration at lower collisionality, observed here on the IR camera, is consistent with previous studies of ELM time scales [7].

This brings the main point of this work. Which reasons stand out as potential causes for the discrepancy between simulations and experiments at higher pedestal pressure? Some of these potential explanations have been identified and should be discussed. Among them, the main ones are: the parallel conductivity model, the SOL temperature level, the divertor boundary conditions, the kinetic effects at lower collisionality, and the pre-ELM pedestal pressure profiles.

Although Braginskii may not be the most advanced model, there is some incentive that this is not the only cause for the observed discrepancy. In previous works [1], it has been shown that using the same equilibrium (i.e. the same ballooning-unstable pressure profiles) at different collisionality reproduces this key feature of ELM dynamics: shorter, more intense ELMs with higher W_{ELM} at lower $\nu_{\mathrm{e}*}^{\mathrm{ped}}$. However, these

previous ELMs were much smaller ($\Delta W_{\mathrm{ELM}} < 2\%$), and the consequence on parallel transport might not be negligible. Note that fluid simulations with 2D CFD codes like EDGE2D-EIRENE or the integrated codes like JINTRAC, which also both assume Braginskii SOL models for the parallel conductivity (with kinetic flux limiting factors), do in fact always overestimate the deposited heat flux at the targets, which is contrary to our result [26, 27]. This strongly suggests that the underestimation of heat fluxes from the present simulations do not come from the Braginskii parallel conduction model, but rather from another aspect of the way these particular JET simulations have been set up.

The temperature level in the SOL can also affect the divertor heat fluxes, since the parallel transport of energy is subject to the sound speed, which depends on the squared root of temperature. In the present set of simulations, a fixed ratio of $T_{\mathrm{AXIS}}/T_{\mathrm{SOL}} = 200$ was assumed for all pulses. Studies with the lithium beam diagnostic and reciprocating Langmuir probes on JET could be used to provide an estimate for the SOL temperature levels depending on other plasma parameters for future simulations [33, 34]. This should determine whether the discrepancy in simulations was due to the assumption for T_{SOL} in the present study. Likewise, more elaborate divertor boundary conditions could be important with respect to the discrepancy between simulations and experiments, and sheath conditions and/or kinetic effects should be included in further studies [13, 28].

One of the main differences, however, in this set of simulations compared to previous works (where the peak divertor heat flux increased at lower $\nu_{\mathrm{e}*}^{\mathrm{ped}}$ [1]) is that each simulated pulse here has its own reconstructed n_{e} and T_{e} profiles. Whereas in this previous study [1], the collisionality scan was done for a fixed pressure profile (hence the same ideal ballooning stability level for all $\nu_{\mathrm{e}*}^{\mathrm{ped}}$ cases). A valid explanation for the discrepancy would be that an advanced EFIT version should be used to map the HRTS profiles. Improved EFIT equilibria that include edge currents would have different flux expansions in the pedestal, which could affect the pressure gradient of ψ-mapped HRTS profiles. Hence, this study should be reproduced with pressure profiles constructed using improved EFIT equilibria.

If the above modifications do not resolve the discrepancy observed at low collisionality, then it means that ELMs cannot be consistently simulated by starting with pre-ELM profiles (i.e. simulations must go through the stability limit of the pressure gradient as in the experiments, which is equivalent to simulating multiple ELM cycles). Note that the simulation of multiple-ELM cycles will be required in any case for the prediction of ELMs in future devices, for which pressure profiles are of course not available. Pre-ELM profiles simulations can only be used for validation against current experiments, not for prediction.

Also, the missing recycling in the present JOREK simulations does lead to an underestimate of the temperature gradients along field lines in the SOL, hence underestimating the conducted heat flow, included in codes like JINTRAC [27]. A reduced MHD model including neutrals (with recycling, charge exchange and radiation) is available for JOREK and has been used for disruption simulations [35]. This model should be used for further ELM studies to include high-recycling divertor conditions which are particularly ITER-relevant. This would solve the problem of higher parallel gradients in the SOL and induced larger parallel heat fluxes, as in [27].

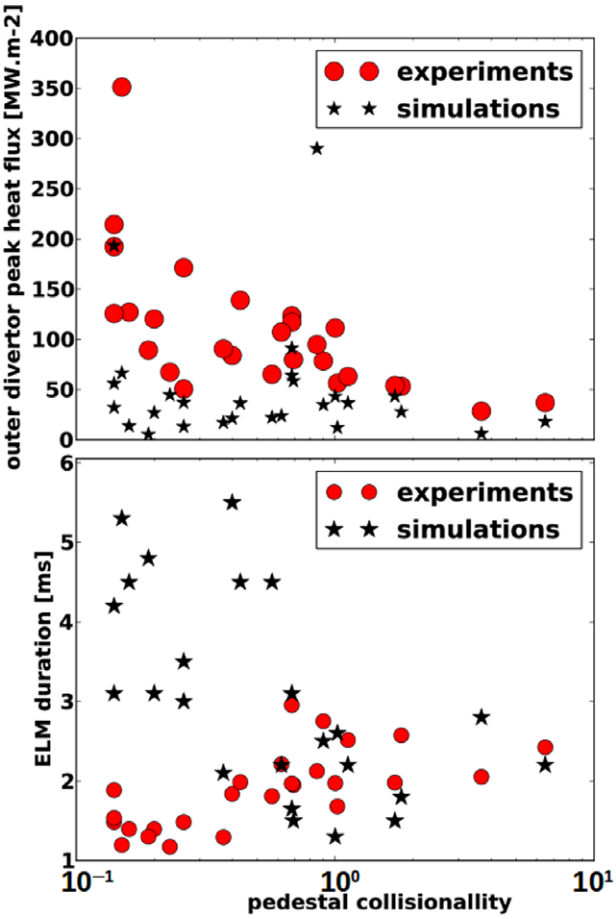

Figure 8. Heat flux and ELM duration as a function of pedestal collisionality.

Kinetic effects at low collisionality and low resistivity could also be important for simulations of ELM energy losses, as has been shown in past studies [28, 36]. A first approach would be to use modified fluid models as proposed in [28]. The most appropriate solution would be to develop a coupled fluid-kinetic model for the JOREK code. However, since it has not yet been demonstrated by any non-linear 3D fluid code that kinetic corrections are absolutely necessary to reproduce experimental observations of ELM-induced heat fluxes at low collisionality, effort should be focused on improving the present fluid simulations before going to more elaborate models. In other words, the step toward a significantly more complex (and more challenging) physics model should only be taken once fluid models have been thoroughly understood and mastered.

Finally, and most importantly, it should be noted that one obvious possibility for the discrepancy could be that only single-harmonic simulations have been produced, and that multi-mode simulations could involve mode-coupling and thus higher MHD activity [24]. Simulations using $n = 1,\ldots,8$ and

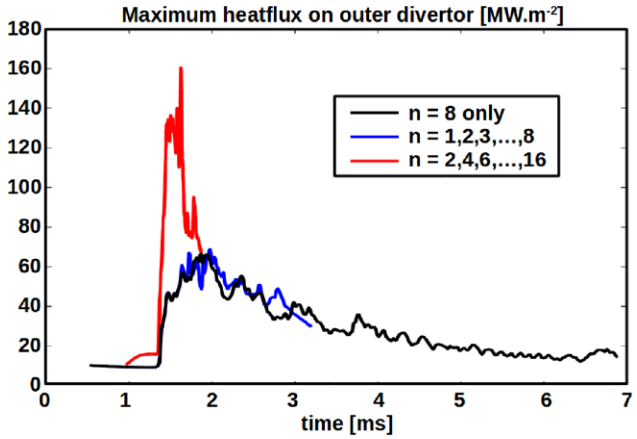

Figure 9. Simulations for JET pulse 83334 (one of the high pedestal pressure cases) with three different sets of toroidal resolutions. With $n = 8$ only (black), with all modes $n = 1$, 2, 3,...,8, and with even modes $n = 2$, 4, 6,...,16. It can be seen that lower mode numbers do not influence the divertor heat fluxes, but coupling with higher mode numbers, however, results in over a factor 2 increase in maximum divertor heat flux. Such simulations will be run in the future for all pulses to check if this resolves the discrepancy observed at low collisionality.

$n = 2,4,6,\ldots,16$ have been run for one of the cases at high pedestal pressure. In the early phase of the crash, the peak heat flux on the outer divertor remains close to the single-harmonic case, it is in fact slightly lower for the case $n = 2,4,6,\ldots,16$. In the later phase, however, non-linear coupling between modes occurs, and although it has little effect for the case $n = 1,\ldots,8$, it is not negligible for the case $n = 2,4,6,\ldots,16$, where the peak heat flux is over a factor 2 higher than the single harmonic case. Figure 9 shows the evolution of the peak heat flux for the three cases, single harmonic, $n = 1,\ldots,8$ and $n = 2,4,6,\ldots,16$. In the future, multi-harmonic simulations will be run for all pulses, to evaluate the extent of single harmonic simulations on ELM, and if single-mode simulations should not be used to describe coherent ELM crashes. At present, it is inadequate to propose any global conclusion based on this simulation for one pulse, in particular, whether this would solve the discrepancy observed at low collisionality or not.

6. Conclusion and discussion

In order to start systematic comparison of ELM simulations against experimental data, a preliminary database of JET ILW unseeded pulses has been built. In future years, such databases on past and current tokamak devices will enable the validation of non-linear MHD codes like JOREK and thus provide confidence with regards to predictions of ELM energy losses and divertor heat loads in future fusion machines like ITER and DEMO.

A first set of simulations was produced using these JET pulses, and results were compared to previous simulations and to experimental observations. By lowering viscosity as well as resistivity to experimentally-relevant values, significant progress has been achieved with respect to previous results. In particular, it has been shown that non-linear MHD can reproduce long ELM crashes of several ms with energy losses comparable to experimental observations. Also, ELM precursors have been obtained for some of the pulses simulated, which is evidence that simulations are coming closer to experimental conditions.

However, although the ELM energy losses seem to be consistent with experiments, the way in which energy is transported from the pedestal to the divertor is not reproduced accurately at lower pedestal collisionality levels that are most ITER-relevant. Some candidates have been proposed to possibly explain the cause of this discrepancy. The first is the Braginskii parallel conductivity model, which could be insufficient to describe pedestal and SOL parallel transport during ELMs. Ideally a kinetic model would be necessary, and coupled fluid-kinetic models should be developed in the future. In any case, for numerical stability, the level of the Braginskii coefficients in simulations was lower than the theoretical values for electron temperature, which should be improved in order to reproduce the high heat flux patterns observed with the IR divertor camera. The second possible reason for the lower heat fluxes at low collisionality is that the SOL temperature levels in the simulations were not chosen consistently with experimental studies, which could significantly affect the sound speed in the SOL, and hence the parallel transport of energy. The third solution would be to use more elaborate models for the divertor boundary conditions, since in the present study only Bohm boundary conditions were used. The fourth possible explanation for the discrepancy is that an improved EFIT version should be used to map the pre-ELM HRTS profiles that are used in simulations. Edge bootstrap current, which is ignored in the standard magnetic-only EFIT on JET, could affect the poloidal magnetic flux expansion in the pedestal, and therefore have repercussions on the ψ-mapped HRTS pedestal gradients. Advanced EFIT versions are currently under development and more consistent HRTS profiles should be achievable in the coming year. Alternatively, AUG simulations should also be undertaken, since the CLISTE equilibrium code has been shown to be in remarkable agreement with diagnostics [37].

One clear caveat in the simulations presented here are that a single mode number has been used. Simulations with multiple mode numbers and non-linear coupling between modes could also solve the discrepancy at low collisionality, although this cannot be confirmed until multiple-mode simulations have been produced for all pulses.

These issues—the parallel conductivity model, the SOL temperature, the divertor boundary conditions, improved EFIT equilibria for the HRTS mapping, and most importantly multiple-mode numbers simulations—should be approached simultaneously to improve the simulations and their comparison to experiments. However, the possibility remains that none of these improvements would ameliorate the discrepancy at high pedestal pressure. This would be a strong indication that only simulations of multiple ELM cycles can reproduce the ELM crashes accurately, in which case simulations with diamagnetic effects, low resistivity and low viscosity should become the main focus of efforts. This is the reason why the presence of precursors in some simulations represents a major result here, since precursors are a key experimental aspect of

the evolution of the pedestal pressure gradient through the ballooning stability limit.

This intermediate step—the simulation of a preliminary database of discharges—is critical since its success is required before large scale simulations of several hundred pulses can be attempted, which would represent significant computational time and cost, and will be necessary in the coming years.

Acknowledgments

This work has been carried out within the framework of the EUROfusion Consortium and has received funding from the Euratom research and training programme 2014–2018 under grant agreement No 633053, and from the RCUK Energy Programme [grant number EP/I501045]. To obtain further information on the data and models underlying this paper please contact PublicationsManager@ccfe.ac.uk. A part of this work was carried out using the HELIOS supercomputer system (IFERC-CSC), Aomori, Japan, under the Broader Approach collaboration, implemented by Fusion for Energy and JAEA. The views and opinions expressed herein do not necessarily reflect those of the European Commission or the ITER Organization.

References

[1] Pamela S *et al* 2011 *Plasma Phys. Control. Fusion* **53** 054014
[2] Pamela S *et al* 2013 *Plasma Phys. Control. Fusion* **55** 095001
[3] Orain F *et al* 2015 *Plasma Phys. Control. Fusion* **57** 014020
[4] Pamela J *et al* 2007 *J. Nucl. Mater.* **363–365** 1–11
[5] Matthews G *et al* 2013 *J. Nucl. Mater.* **438** S2–10
[6] Beurskens M *et al* 2009 *Nucl. Fusion* **49** 125006
[7] Frassinetti L *et al* 2015 *Nucl. Fusion* **55** 023007
[8] Frassinetti L *et al* 2012 *Rev. Sci. Inst.* **83** 013506
[9] Eich T *et al* 2009 *J. Nucl. Mater.* **390–391** 760
[10] Sieglin B *et al* 2013 *Plasma Phys. Control. Fusion* **55** 124039
[11] Huysmans G and Czarny O 2007 *Nucl. Fusion* **47** 659–66
[12] Czarny O and Huysmans G 2008 *J. Comput. Phys.* **227** 7423–45
[13] Huijsmans G and Loarte A 2013 *Nucl. Fusion* **53** 123023
[14] Huijsmans G *et al* 2015 *Phys. Plasmas* **22** 021805
[15] Orain F *et al* 2013 *Phys. Plasmas* **20** 102510
[16] Becoulet M *et al* 2012 *Nucl. Fusion* **52** 054003
[17] Strauss H 1976 *Phys. Fluids* **19** 134
[18] Strauss H 1997 *J. Plasma Phys.* **57** 83–7
[19] Braginskii S I Transport processes in a plasma *Reviews of Plasma Physics* vol 1 (London: Springer) pp 205–311
[20] Saarelma S *et al* 2013 *Nucl. Fusion* **53** 123012
[21] Kallenbach A *et al* 2005 *J. Nucl. Mater.* **337–339** 381–5
[22] Sauter O *et al* 1999 *Phys. Plasmas* **6** 2834
[23] Futatani S *et al* 2014 *Nucl. Fusion* **54** 073008
[24] Krebs I *et al* 2013 *Phys. Plasmas* **20** 082506
[25] Orain F *et al* 2015 *Phys. Rev. Lett.* **114** 035001
[26] Harting D *et al* 2014 *J. Nucl. Mater.* **463** 493–7
[27] Wiesen S *et al* 2011 *Plasma Phys. Control. Fusion* **53** 124039
[28] Tskhakaya D *et al* 2008 *Contrib. Plasma Phys.* **48** (1–3) 83–93
[29] Moulton D *et al* 2013 *Plasma Phys. Control. Fusion* **55** 085003
[30] Webster A *et al* 2012 *Nucl. Fusion* **52** 114023
[31] Pamela S *et al* 2010 *Plasma Phys. Control. Fusion* **52** 075006
[32] Havlickova E *et al* 2014 *Plasma Phys. Control. Fusion* **56** 075008
[33] Brix M *et al* 2012 *Rev. Sci. Instrum.* **83** 10D533
[34] Silva C *et al* 2009 *Plasma Phys. Control. Fusion* **51** 105001
[35] Fil A *et al* 2015 *Phys. Plasmas* **22** 062509
[36] McClements K and Thyagaraja A 2004 *Plasma Phys. Control. Fusion* **46** 39–60
[37] Dunne M *et al* 2015 *Nucl. Fusion* **55** 013013
[38] Romanelli F 2014 *Proc. of 25th IAEA Fusion Energy Conf. (Saint Petersburg, Russia, 2014)*